Zeitschrift: Helvetica Physica Acta
Band: 58 (1985)
Heft: 2-3

Artikel: Theory of the resonant Raman scattering by two phonons in germanium and silicon
Autor: Cardona, Manuel / Allen, Philip B.
DOI: https://doi.org/10.5169/seals-115600

Helvetica Physica Acta, Vol. 58 (1985) 307–320 0018–0238/85/020307–14$1.50 + 0.20/0

Theory of the resonant Raman scattering by two phonons in germanium and silicon

By Manuel Cardona and Philip B. Allen,[1]) Max-Planck-Institut für Festkörperforschung, Heisenbergstrasse 1, 7000 Stuttgart 80, Federal Republic of Germany

(30. VIII. 1984)

In honor of Emanuel Mooser's 60th birthday

Abstract. Resonant Raman scattering by two phonons has been observed near the E_0' and E_1 gaps of Si (3.4 eV) and near the E_1 and $E_1+\Delta_1$ gaps of Ge (2.1 and 2.3 eV). We present here microscopic calculations of the resonance Raman spectra including their scattering efficiencies normalized to that for one phonon scattering. These calculations are based on the bond charge model for the lattice dynamics and the electron–phonon interaction obtained from a local pseudopotential band structure. For simplicity the calculations have been limited to the E_0 and E_0' gaps of Ge and the E_0' gap of Si. The results obtained show considerable agreement with the experimental data. The results of the calculations are recast in the form of average electron–two-phonon deformation potentials.

I. Introduction

The advent of high power cw ion lasers made possible the measurement of two phonon Raman spectra of semiconductors in the visible and near uv, a region in which most of these materials are opaque [1]. In the cases of germanium [2] and silicon [3] a striking correspondence was found between the structure in the two-phonon spectra and critical points in the density of two-phonon overtones [4], especially for the Γ_1 scattering configuration [2, 3].

Further developments in the field of ion lasers and of cw tunable dye lasers enable the measurement of the resonance in the two-phonon spectra for laser frequencies in the neighborhood of critical points (i.e., van Hove singularities) in the electronic interband transition energies. For Ge the spin-orbit-split E_1 and $E_1+\Delta_1$ critical points, which fall in the convenient 2.0–2.4 eV region (see Fig. 1), were investigated [5]. The lowest direct gap was not accessible to the lasers available at that time. For silicon the E_1, $E_1+\Delta_1$ resonance, which is nearly degenerate with E_0' (see Fig. 1), was investigated [6]. In this case the spin-orbit splitting is small ($\Delta_1 \simeq 0.03$ eV): the resulting complex of 3 critical points is henceforth referred to as E_1. The E_1 critical points of Si take place for $\omega \simeq$ 3.4 eV.

An approximate analysis of the observed resonances gave information about the electron-two phonon interaction mechanisms. The results were described in terms of renormalized electron two-phonon deformation potentials D_1, $D_{25'}$, and

[1]) Permanent address: Dept. of Physics, SUNY, Stony Brook, N.Y. 11794, U.S.A.

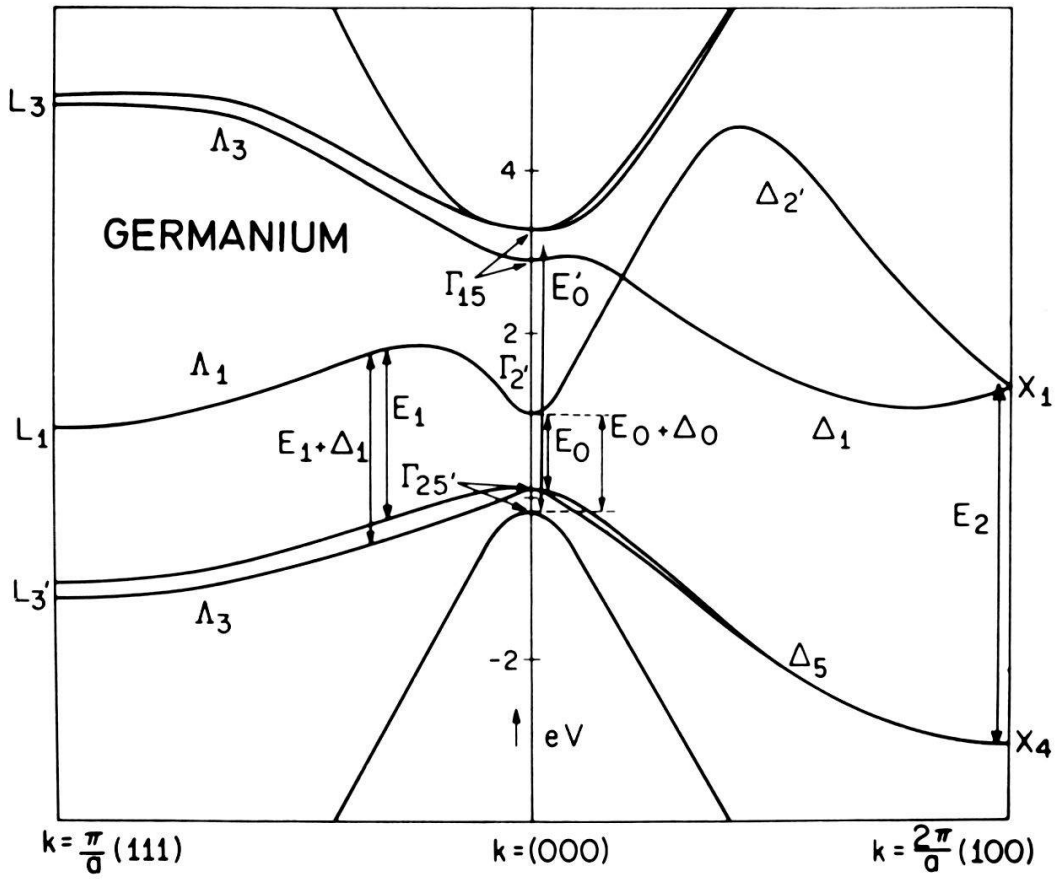

Figure 1
Band structure of germanium showing the E_0, $E_0+\Delta_0$, E_1, $E_1+\Delta_1$, and E_0' critical points. The $X_4 \rightarrow X_1$ transitions contribute to the E_2 structure. From M. Cardona, Modulation Spectroscopy (Academic Press, New York, 1969), p. 66.

D_{12}, for the three irreducible scattering configurations. These renormalized parameters, which in some cases turn out to be rather large [7], contain the intrinsic electron–two-phonon matrix element and the effect of the electron–one-phonon interaction taken in second order perturbation theory. The resonance enhancement observed for the two-phonon spectra was usually similar to that of the first-order spectrum [6] with the exception of a stronger resonance observed for two optical phonons with wave vector $q \simeq 0$. In this case the renormalization just described may (in principle) fail.

Here we present microscopic calculations of the two-phonon Raman spectra of Ge and Si in the strongly resonant regime of laser frequency $\omega_L \simeq \omega_g$, where ω_g is taken to be the E_0' gap of Ge and Si (spin-orbit splitting neglected) and the E_0 gap of Ge. The three irreducible components of these spectra ($\Gamma_1, \Gamma_{25'}, \Gamma_{12}$) are calculated. The scattering efficiencies are given relative to that for one-phonon scattering. The results show clearly the stronger resonance observed experimentally for two optical phonons with $q \simeq 0$. Comparison with experimental data is not straightforward since these data were obtained near gaps which were easily accessible to experiment but do not coincide with the gaps at $k = 0$, easily accessible to theory. Nevertheless a striking correlation between the shapes of the measured and calculated spectra is found. Also, the observed scattering efficiencies agree with the calculations, provided they are normalized to that for one-phonon scattering. Apparently this normalization process removes strength factors which are common to both first and second-order scattering mechanisms.

II. Theory

Most of the available calculations of second-order Raman spectra are based on bond polarizability models (see Ref. 8 for Ge and Si). These models cannot account for details of electronic resonance effects. We present here the results of calculations based on Weber's bond charge model for the lattice dynamics [4] and the microscopic pseudopotential model for the electron–phonon interactions used in Ref. 9 to calculate the temperature dependence of the band structure. The calculations are restricted to the E_0 and E_0' gaps of Ge and the E_0' gap of Si (see Fig. 1). This restriction to $k=0$ gaps cuts down on computer time since the calculation can be restricted to the reduced Brillouin zone (1/48 of the full zone). Extension to the experimentally popular E_1 gaps (Fig. 1) would increase the required time by about a factor of 6. The electron–phonon interaction is calculated on the basis of the empirical pseudopotential band structure model of Bergstresser and Cohen [10] which does not include spin-orbit interaction. This represents no restriction for Si where spin-orbit splittings cannot be resolved. In the case of Ge the spin-orbit splittings can be reliably introduced "by hand" after performing the numerical calculation. Our calculations are confined to $T=0$ K. Although most of the experiments were performed for $T\approx 300$ K, a generalization to higher temperatures involves first of all a trivial multiplication of the spectra calculated at $T=0$ by the temperature dependent Bose–Einstein factor:

$$\begin{aligned}
&1+n(\omega_R) \text{ for first-order Stokes scattering,}\\
&[1+n(\omega_{R1})][1+n(\omega_{R2})] \text{ for second-order Stokes scattering,}\\
&n(\omega)=[\exp(\hbar\omega/k_BT)-1]^{-1}. \qquad (1)
\end{aligned}$$

There is also a small mixed Stokes-antistokes term which can usually be neglected. At finite temperature the gaps must also be broadened and usually down shifted with respect to those for $T=0$ [9, 11, 12]. We should mention that it is not clear whether the same renormalization, as occurs in the dielectric function [13], applies also to the gaps observed in resonant Raman scattering [5]. In any case these renormalizations are small and should not affect the comparison of our calculations with experiment provided one stays in both cases close to the peak in the resonance.

Our calculations also assume that all phonon frequencies are smaller than the Lorentzian broadenings of the electronic critical points which at room temperature amount to 50 meV for the E_1 gap of Ge [12] and 80 meV for that of Si. In fact, for the purpose of eliminating noise due to the finite mesh size of our Brillouin zone integrations, a Lorentzian broadening of 100 meV was used in all our calculations.

The Feynman diagrams which are responsible for first and second order scattering in a model involving uncorrelated electrons [15] are shown in Fig. 2. The renormalization of the electron two-phonon vertex of Fig. 2c and d is described in Fig. 2f. It corresponds to the intrinsic electron-two phonon interaction plus the electron-one-phonon interaction taken to second order. It can be easily seen that the term in Fig. 2e is negligible close to resonance. We should mention that the electron-phonon parts of diagrams c and d also give the electron self-energy if one phonon is emitted and the other absorbed [9]. Hence most of the theory in Ref. 9 can be easily taken over for the calculation of the second order Raman scattering (see also equation (2.243) of Ref. 1). One must simply

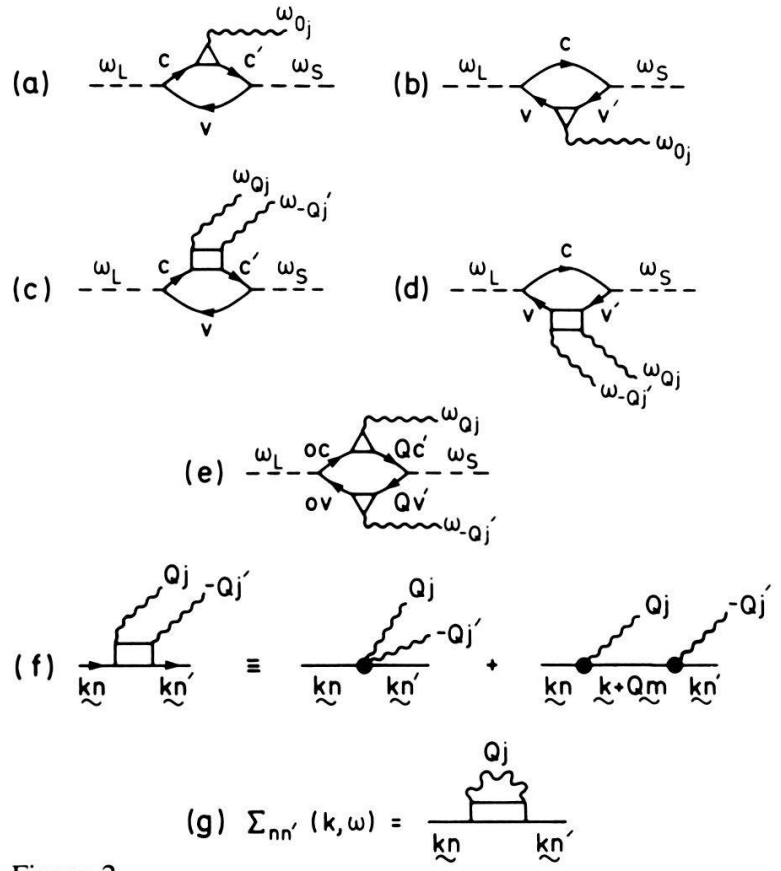

Figure 2

(a) and (b) represent first-order Raman processes; (c) and (d) are the second-order processes important near resonance where (e) is negligible (because less resonant); (f) shows the effective electron-two phonon vertex; (g) shows the self energy which gives the temperature renormalization of the bands and which is closely related to the $j = j'$ electron-two phonon vertex.

multiply the diagrams responsible for the temperature dependence of electronic states by the electron-photon interaction vertices and square before summing over the Brillouin zone. Since the effect of these vertices at resonance is basically the same for diagrams (a, b) as for (c, d), they disappear when taking the ratio of second to first order scattering efficiencies.

The efficiency (i.e., scattering probably per unit path length, per unit scattered frequency ω_R and unit solid angle Ω) for either first or second order scattering is given by (see (2.55) of Ref. 1):

$$\frac{\partial^2 S^{(n)}}{\partial\Omega\,\partial\omega_R} = \left(\frac{\omega_S}{c}\right)^4 I^{(n)}_{\alpha\beta\gamma\delta}\hat{e}_{L\alpha}\hat{e}_{L\gamma}\hat{e}_{S\beta}\hat{e}_{S\delta}, \tag{2}$$

where ω_S is the scattered frequency, c the speed of light in vacuum, and the unit vectors $\hat{e}_{L,S}$ represent the polarization of the laser and scattered beam. The tensor $I^{(n)}_{\alpha\beta\gamma\delta}$ represents the fluctuations of the polarizability which correspond to the scattering channel under consideration, and n indicates the number of phonons involved in the process. The tensors $I^{(1)}_{\alpha\beta\gamma\delta}$ can be expressed as a function of the first order Raman tensors $a^{(1)}_{\alpha\beta}$ as:

$$I^{(1)}_{\alpha\beta\gamma\delta} = \sum_j a^{(1)}_{\alpha\beta}a^{(1)}_{\gamma\delta}\delta(\omega_R - \omega_{0j}) \tag{3}$$

$$a^{(1)}_{\alpha\beta} = \sum_{\mathbf{k}cc'vv'} \chi'_{\alpha\beta}(\mathbf{k}vv'cc')[\delta_{cc'}\Delta^{(1)}_j(\mathbf{k}v, \mathbf{k}v') - \delta_{vv'}\Delta^{(1)}_j(\mathbf{k}c, \mathbf{k}c')] \tag{4}$$

where $\Delta_j^{(1)}(s, s')$ represents the matrix element for electron scattering from $|s\rangle$ to $|s'\rangle$ by an optic phonon of branch j

$$\Delta_j^{(1)}(s, s') = \langle s| H_{ep}^{(1)}(j) |s'\rangle$$
$$= \left(\frac{\hbar}{2MN\omega_{0j}}\right) \sum_{\kappa} e_{\mu}(oj, \kappa)\langle s| \partial V/\partial R_{\mu}(\kappa) |s'\rangle. \tag{5}$$

$\hat{\varepsilon}(\mathbf{Q}j, \kappa)$ is the phonon polarization vector on the κth atom in the unit cell, N is the number of unit cells, and V is the pseudopotential. The "differential susceptibilities" χ' are given by:

$$\chi'_{\alpha\beta}(\mathbf{k}vv'cc') = \frac{e^2\hbar^2}{m} r_{\alpha}(\mathbf{k}vc) r^*_{\beta}(\mathbf{k}v'c')$$
$$r_{\alpha}(\mathbf{k}vc) = \langle \mathbf{k}v |p_{\sigma}| \mathbf{k}c\rangle/(\varepsilon_{\mathbf{k}c} - \varepsilon_{\mathbf{k}v})(\hbar\omega - \varepsilon_{\mathbf{k}c} + \varepsilon_{\mathbf{k}c}). \tag{6}$$

They are related to the usual susceptibility χ by

$$\frac{d\chi}{d\omega} = \sum_{\mathbf{k}vc} \chi'(\mathbf{k}vvcc). \tag{7}$$

Likewise $I^{(2)}_{\alpha\beta\gamma\delta}$ can be written as:

$$I^{(2)}_{\alpha\beta\gamma\delta} = 2 \sum_{\vec{Q}jj'} a^{(2)}_{\alpha\beta}(\mathbf{Q}jj') a^{(2)}_{\gamma\delta}(\mathbf{Q}jj') \delta(\omega_R - \omega_{\mathbf{Q}j} - \omega_{\mathbf{Q}j'}) \tag{8}$$

with j representing the six phonon branches and $\vec{Q}$ the wavevector of one of the phonons involved in the process. The Raman tensor $a^{(2)}_{\alpha\beta}$ becomes:

$$a^{(2)}_{\alpha\beta}(\mathbf{Q}, jj') = \sum_{\mathbf{k}vv'cc'} \chi'_{\alpha\beta}(\mathbf{k}vv'cc')[\delta_{cc'}\Delta^{(2)}_{\mathbf{Q}jj'}(\mathbf{k}v, \mathbf{k}v') - \delta_{vv'}\Delta^{(2)}_{\mathbf{Q}jj'}(\mathbf{k}c, \mathbf{k}c')], \tag{9}$$

where $\Delta^{(2)}_{\mathbf{Q}jj'}(s, s')$ is the effective electron-two phonon matrix element for scattering from $|s\rangle$ to $|s\rangle$ by two phonons $(\mathbf{Q}j, -\mathbf{Q}j')$

$$\Delta^{(2)}_{\mathbf{Q}jj'}(s, s') = \langle s| H^{(2)}_{ep}(\mathbf{Q}j, -\mathbf{Q}j') |s'\rangle. \tag{10}$$

From the rigid pseudopotential model we get the explicit formula

$$\Delta^{(2)}_{\mathbf{Q}jj'}(\mathbf{k}n, \mathbf{k}n') = \sum_{\kappa\kappa'} \left(\frac{\hbar^2}{4M^2\omega_{\mathbf{Q}j}\omega_{\mathbf{Q}j'}}\right)^{1/2} e_{\mu}(\mathbf{Q}j, \kappa) e^*_{\nu}(\mathbf{Q}j', \kappa)$$
$$\times \left\{ e^{i\mathbf{Q}\cdot(\tau_{\kappa} - \tau_{\kappa'})} \frac{\langle \mathbf{k}n| \partial V/\partial R_{\mu}(\kappa) |\mathbf{k} + \mathbf{Q}m\rangle\langle \mathbf{k} + \mathbf{Q}m| \partial V/\partial R_{\nu'}(\kappa') |\mathbf{k}n'\rangle}{\varepsilon_{\mathbf{k}n} - \varepsilon_{\mathbf{k}+\mathbf{Q}m} - \hbar\omega_{\mathbf{Q}j}} \right.$$
$$\left. - \frac{\langle \mathbf{k}n| \partial V/\partial R_{\mu}(\kappa) |\mathbf{k}m\rangle\langle \mathbf{k}m| \partial/\partial R_{\nu}(\kappa') |\mathbf{k}n'\rangle}{\varepsilon_{\mathbf{k}n} - \varepsilon_{\mathbf{k}m}} \right\}. \tag{11}$$

In equation (11) we have used translational invariance to transform the matrix element of the second order electron–phonon interaction into the second term in curly brackets (see Ref. 9). Equations (3–11) give a prescription to calculate the first and second order Raman scattering which becomes manageable in the neighborhood of a resonance at $\vec{k} = 0$. The only independent component of $a^{(1)}_{\alpha\beta}$ is $a^{(1)}_{xy}$ since the Raman phonon has $\Gamma_{25'}$ symmetry. For $a^{(2)}_{\alpha\beta}$ we must calculate three

independent components, namely:

$$a^{(2)}_{\Gamma_1} = \tfrac{1}{3}\sum_{\alpha} a^{(2)}_{\alpha\alpha}$$
$$a^{(2)}_{25'} = a^{(2)}_{xy} \tag{12}$$
$$a^{(2)}_{\Gamma_{12}} = \frac{1}{2\sqrt{3}}(a^{(2)}_{xx} - a^{(2)}_{yy}).$$

Near the $\vec{k} = 0$ gaps the difficult $\vec{k}$ integration involved in equations (4) and (9) can be avoided if one assumes that the matrix elements $\Delta^{(n)}$ of these equations are independent of $\vec{k}$, an assumption which is justified since the main contribution to $a^{(1)}$ comes from $\vec{k} \simeq 0$ because of the singularity of χ' at resonance.

We shall work out the first order answer at an E_0 gap. The $\Gamma_{2'}$ conduction band is singly degenerate and cannot couple to the $\Gamma_{25'}$ Raman phonon ($\Delta^{(1)}_j(0c, 0c) = 0$). The $\Gamma_{25'}$ valence band is triply degenerate and is spanned by states of the symmetry type:

$$|1\rangle = |yz\rangle$$
$$|2\rangle = |zx\rangle \tag{13}$$
$$|3\rangle = |xy\rangle.$$

In this basis, we have

$$\Delta^{(1)}_z(0v, 0v') = \Delta^{(1)}\begin{pmatrix} 0 & 1 & 0 \\ 1 & 0 & 0 \\ 0 & 0 & 0 \end{pmatrix},$$

where the $j = z$ phonon is polarized in the $\hat{z}$ direction. Following a convention established by Lawaetz [16], the coupling matrix element in diamond structure is

$$\Delta^{(1)} = \sqrt{3}\, d_0(u/a) \qquad u = (\hbar/4MN\omega_{0j})^{1/2}, \tag{14}$$

where a is the lattice constant, u is the atomic displacement amplitude, and d_0, the optic phonon deformation potential, as calculated from equation (5) has the values (34.9 eV, 38.2 eV) in (Si, Ge). According to equation (4) the only element of χ needed is $\chi'_{xy}(\mathbf{k}, 1, 2, c, c)$ which by symmetry is the same as $\chi'_{xx}(\mathbf{k}, 1, 1, c, c)$. Thus we can exploit equation (7) and find for equation (4) at $\omega \simeq E_0$

$$a^{(1)}_{xy}(E_0) = \left(\frac{d\chi}{d\omega}\right) - \frac{\sqrt{3}\, d_0}{a}\left(\frac{\hbar}{4MN\omega_{0j}}\right)^{1/2}. \tag{15}$$

When spin-orbit effects are introduced, this result evolves into equation (2.195) of Ref. 1. For an E'_0 gap the Γ_{15} conduction band state now interacts with the Raman phonon. This simply results in d_0 being replaced by d_0–d_{15}, where d_{15} is the optic deformation potential for Γ_{15} valence band states, which we find to be (−16.5 eV, −18.4 eV) for (Si, Ge). Our values of d_0 and d_{15} agree closely with those of Blacha *et al.* [17].

Our procedure for calculating $a^{(2)}_{\alpha\beta}$ is to avoid the $\mathbf{k}$ sum in equation (9) in a

manner similar to that of equation (15):

$$a^{(2)}_{\alpha\beta} \cong \frac{d\chi}{d\omega} \sum_{vv'cc'} r_{\alpha\beta}(vv'cc')[\delta_{cc'}\Delta^{(2)}_{\mathbf{Q}jj'}(0v, 0v') - \delta_{vv'}\Delta^{(2)}_{\mathbf{Q}jj'}(0c, 0c')] \tag{16}$$

$$r_{\alpha\beta}(vv'cc') = d_v d_c \langle 0v|\, p_\alpha\, |0c\rangle\langle 0c'|\, p_\beta\, |0v'\rangle / \sum_{vc} \langle 0v|\, p_x\, |0c\rangle|^2, \tag{17}$$

where $d_{v,c}$ is the degeneracy.

III. Results

We calculate using equations (3–11, 15–17) the ratios

$$\begin{aligned} R_{\Gamma_1}(\omega_R) &= \frac{I^{(2)}_{1111} + 2I^{(2)}_{1122}}{3\,|a^{(1)}_{12}|^2} \\ R_{\Gamma_{25'}}(\omega_R) &= \frac{I^{(2)}_{1212}}{|a^{(1)}_{12}|^2} \\ R_{12}(\omega_R) &= \frac{I^{(2)}_{1111} - I^{(2)}_{1122}}{6\,|a^{(1)}_{12}|^2} \end{aligned} \tag{18}$$

as a function of the Raman shift ω_R at the E_0 and E_0' gap of Ge and at the E_0' gap of Si. In taking these ratios near resonance, the divergences in the energy denominators of χ' (equation (6)) disappear. Consequently, the result becomes nearly independent of laser frequency except for the first energy denominator in equation (11) which vanishes for $Q = 0$. Hence a strong enhancement is expected for scattering by overtones of the Raman phonon.

In evaluating the matrix elements of the electron–phonon interaction for arbitrary Q we need the pseudopotential form factors $V(Q)$ for all Q's. However, only the $V(Q)$'s for Q equal to a reciprocal lattice vector are known accurately from fits to empirical band structure data [10]. Hence we interpolate these $V(Q)$'s for values of $a/(2\pi)Q$ between $\sqrt{3}$ and $\sqrt{12}$; for $a/(2\pi)Q \geq \sqrt{12}$ we set $V(Q) = 0$ (see Fig. 1 of Ref. 9). A difficulty arises with the extrapolation for $a/(2\pi)Q < \sqrt{3}$. We use two possible choices given in Fig. 1 of Ref. 9. One of them is based on the form factor $V(0) = -\frac{2}{3}E_F$ (E_F = Fermi energy of an electron gas of equivalent valence electron density) which holds for a metallic system. The other is based on the assumption $V(0) = 0$.

In order to check the effect of $V(0)$ on the second order Raman spectra we have performed calculations for the E_0' gap of Si with the two values of $V(0)$ given above. The results for $V(0) = 0$ are shown in Fig. 3 and those for $V(0) = -\frac{2}{3}E_F$ in Fig. 4. The calculated Γ_1 and $\Gamma_{25'}$ spectra are nearly the same. Differences appear for the Γ_{12} spectra which in any case are rather weak. Because of this weakness no experimental data are available for this component of the second order scattering, a fact which prevents us from deciding, in an empirical way, which pseudopotential is more appropriate.

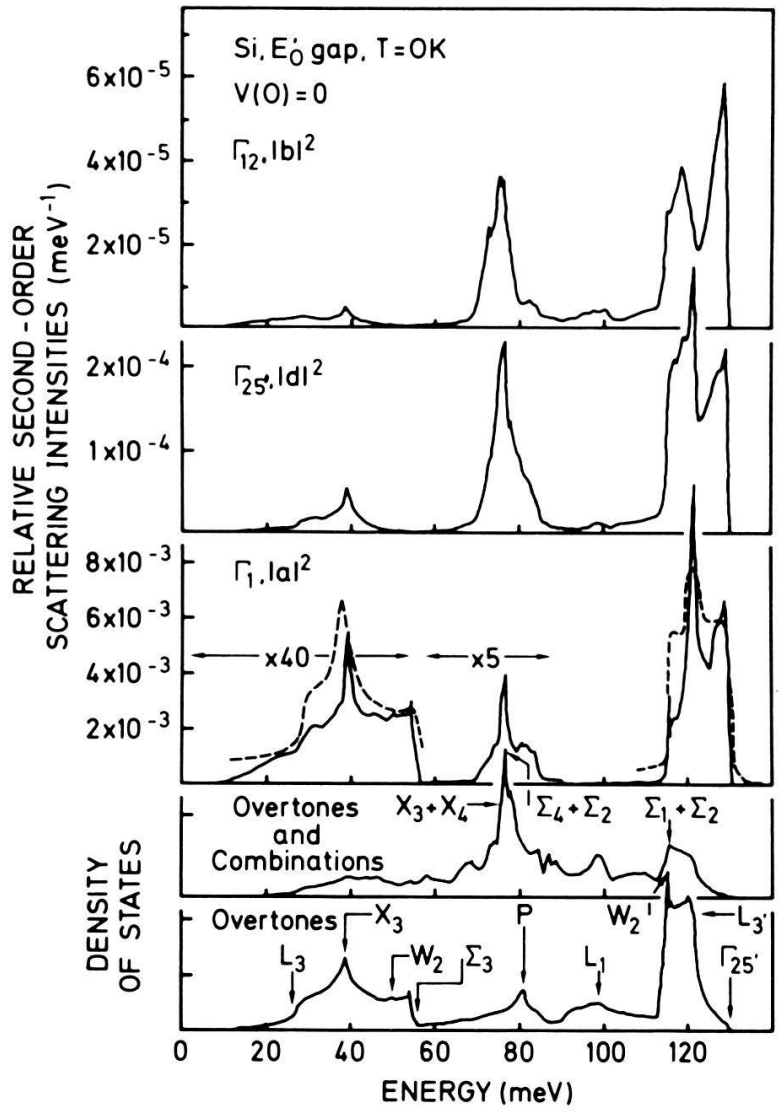

Figure 3
The upper three panels show the calculated Γ_1, $\Gamma_{25'}$, Γ_{12} Raman spectra for Si with the laser photon resonant with the E_0' ($\Gamma_{25'} \rightarrow \Gamma_{15}$) gap. The intensity is normalized to the integrated first order intensity. The electron–phonon coupling is derived from an interpolated local pseudopotential with $V(0) = 0$. The lower two panels give the density of overtone states ($j = j'$) and the total two phonon density of states (all j, j').

Table I shows the total integrated second order scattering efficiencies as a ratio to the integrated first-order efficiencies. The first two rows show that the different extrapolations of the pseudopotential affect the absolute value of the Raman efficiency at a level of 10–20% (which is much greater than the observed 1–2% influence on the calculations of Ref. 9 on the temperature renormalization of the gap). This enhanced sensitivity arises from the fact that second order matrix elements $\langle s| H_{ep}^{(2)}(\mathbf{Q}_j, -\mathbf{Q}_{j'}) |s'\rangle$ are squared before summing over $\mathbf{Q}$ in the Raman case, but not squared for the T-dependence.

For the purpose of assigning the calculated structure in $I_{\alpha\beta\gamma\delta}(\omega_R)$ to van Hove singularities, we show in Figs. 3 and 4 the calculated densities of two-phonon states. Also shown is the measured Γ_1 component [6] after reduction to $T = 0$ (dashed line). These measurements correspond to $\omega_L = 3.41$ eV, a photon energy which lies very close to the E_0' gap ($E_0' = 3.4$ eV for Si). We should bear in

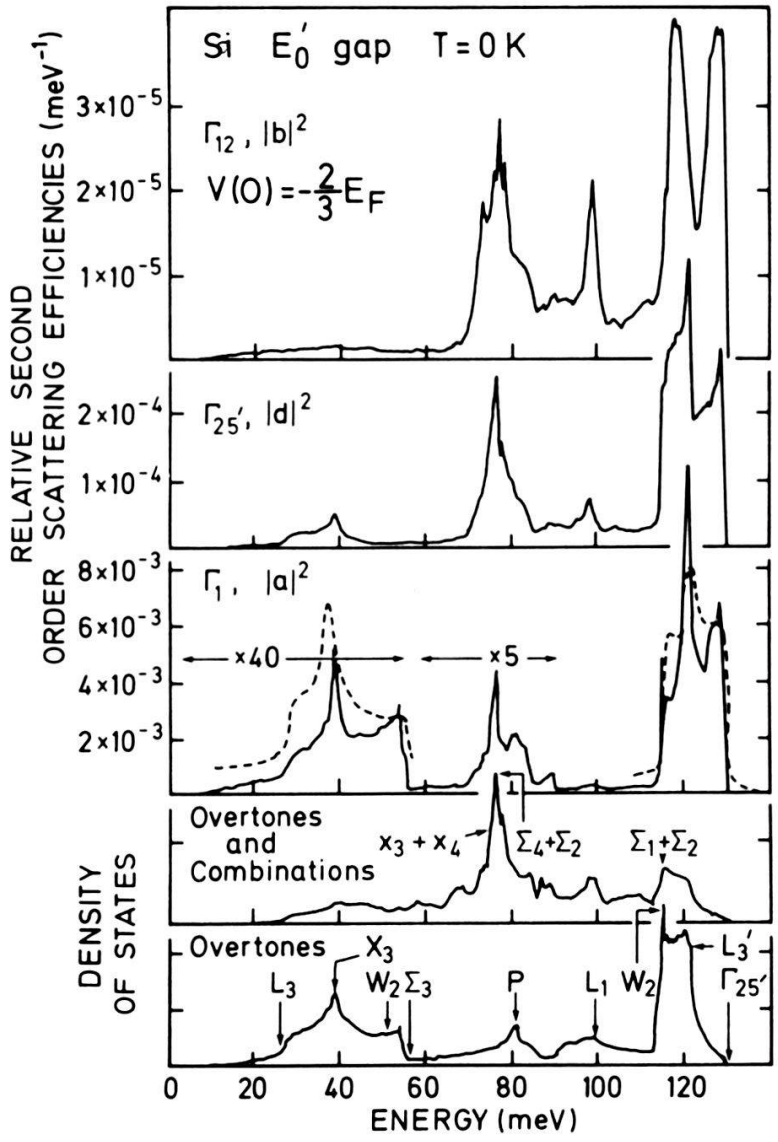

Figure 4
Similar to Fig. 3 except the pseudopotential interpolation uses $V(0) = -2E_F/3$.

mind, however, that the E_0' gap is nearly degenerate with the E_1 gap in Si [10] and that the latter, because of the larger volume of $\vec{k}$-space it spans, must yield the main contribution to the resonant scattering. Nevertheless, the correspondence between the experiment and the calculation is quite good, in particular concerning the ratio of 2TO to 2TA scattering. The main discrepancy concerns

Table I
Integrated second-order Raman efficiencies as a fraction of the integrated first order intensity at the same resonance ($T = 0$). The first two rows show the effect of different extrapolations of the pseudopotential.

		$\Gamma_1, \|a\|^2$	$\Gamma_{25'}, \|d\|^2$	$\Gamma_{12}, \|b\|^2$
Si	$V(0) = 0$	0.082	0.0054	0.00094
E_0' gap	$V(0) = -\frac{2}{3}E_F$	0.091	0.0070	0.00097
Ge	E_0' gap	0.051	0.0079	0.00054
$V(0) = -\frac{2}{3}E_F$	E_0 gap	0.022	0.0056	0.00062

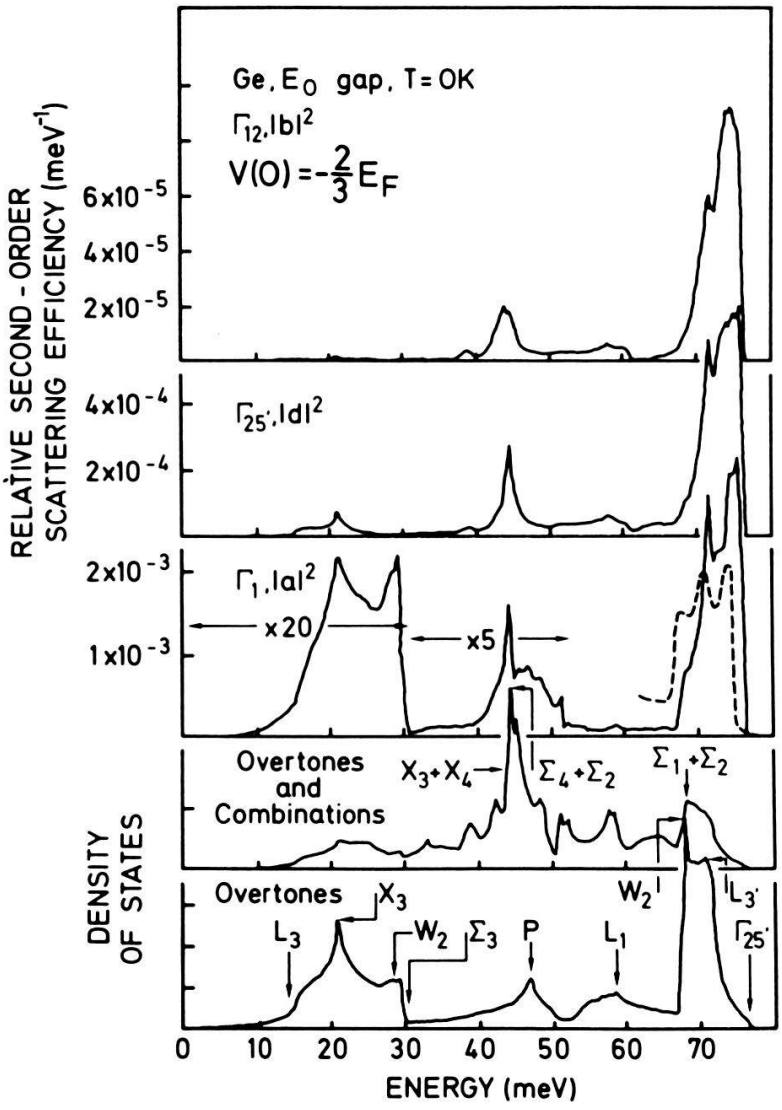

Figure 5
Similar to Fig. 4 except Ge, and the E_0 ($\Gamma_{25'} \rightarrow \Gamma_{2'}$) gap. $V(0) = -2E_F/3$ is used both here and in Fig. 6.

the calculated TA+TO peak which seems to be somewhat stronger than the experimental one [3, 6]. In particular, the experiments reproduce the enhancement in the scattering by overtones of the $\Gamma_{25'}$ optical phonons predicted by the theory.

Figures 5 and 6 show the resonant spectra calculated for the E_0 and the E_0' critical points of Ge for $V(0) = -\frac{2}{3}E_F$. They also display the resonant enhancement of the $2TO(\Gamma_{25'})$ scattering. The experimental data shown in these figures (dashed line) correspond to the E_1 gap (2.2 eV) which in Ge lies between E_0 (0.8 eV) and E_0' (3.1 eV). They also show the resonant enhancement of the $2TO(\Gamma_{25'})$ phonons.

It is desirable to exploit resonant second order Raman scattering to learn experimentally the electron-two phonon coupling strengths. Such work has been reviewed in Ref. 1, especially Table 2.11, with which we now compare our results. A second-order deformation potential D is defined as follows:

$$\langle s|\, H^{(2)}\mathbf{Q}j, -\mathbf{Q}j')\,|s'\rangle = \tfrac{4}{3}D_{s,s'}(\mathbf{Q}jj')\left(\frac{u_{\mathbf{Q}j}}{a}\right)\left(\frac{u_{\mathbf{Q}j'}}{a}\right),$$

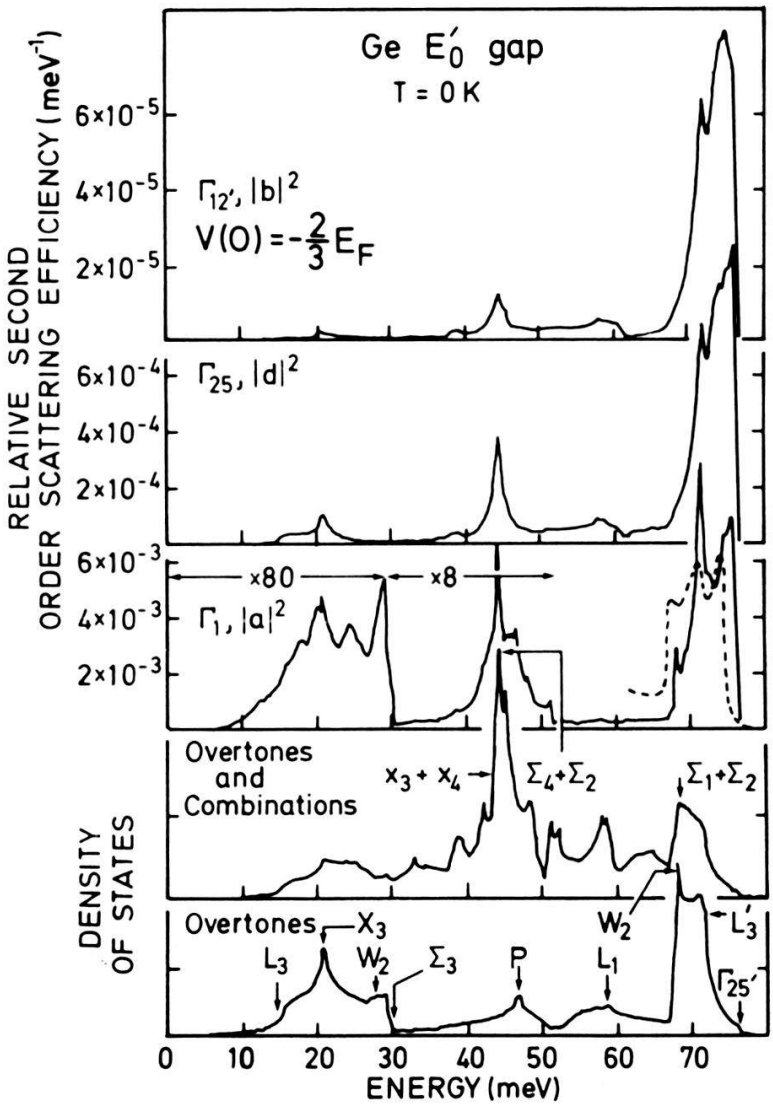

Figure 6
Similar to Fig. 5 except the E_0' ($\Gamma_{25'} \rightarrow \Gamma_{15}$) gap.

where $u_{\mathbf{Q}j}$ is the atomic displacement amplitude given in equation (44). The factor 4/3 is a convention which originated in Ref. 7. Consider again the E_0 gap, and the Γ_1 component of the second-order Raman efficiency, which involves the trace of $a^{(2)}_{\alpha\beta}$ (equation 12). Because of the single degeneracy of the $\Gamma_{2'}$ conduction band state, the trace of $r_{\alpha\beta}$ (equation (17) is $3\delta_{vv'}\delta_{cc'}$, and

$$\tfrac{1}{3}\sum_{\alpha} a^{(2)}_{\alpha\alpha}(E_0) = \frac{4}{3}\frac{d\chi}{d\omega}\left[\sum_{v} D_{vv}(\mathbf{Q}jj') - D_{cc}(\mathbf{Q}jj')\right]\left(\frac{u_{\mathbf{Q}j}}{a}\right)\left(\frac{u_{\mathbf{Q}i}}{a}\right). \tag{19}$$

Let us consider the total Γ_1 Raman intensity in a particular spectral region (e.g., for the "2TO" region between $\omega_1 = 110$ meV and $\omega_2 = 130$ meV in Si). Normalized to the first order intensity, this is (from Eq. (18))

$$A_{\Gamma_1}(\omega_1, \omega_2) \equiv \int_{\omega_1}^{\omega^2} d\omega_R R_{\Gamma_1}(\omega_R). \tag{20}$$

Using equations (18), (8), (15), (19) we get

$$A_{\Gamma_1}(\omega_1,\omega_2)=\frac{8}{27}\frac{\hbar}{MN\omega_0 a^2}\frac{1}{d_0^2}\sum_{\mathbf{Q}jj'}^{\omega_1<\omega_{\mathbf{Q}j}+\omega_{\mathbf{Q}j'}<\omega_2}\left[\sum_{\upsilon}D_{\upsilon\upsilon}(\mathbf{Q}jj')-D_{cc}(\mathbf{Q}jj')\right]^2\frac{\omega_0}{\omega_{\mathbf{Q}j}}\frac{\omega_0}{\omega_{\mathbf{Q}j'}}$$
$$\simeq\frac{8}{27}\left(\frac{\hbar}{M\omega_0 a^2}\right)\frac{\omega_0}{\omega_A}\frac{\omega_0}{\omega_B}n_p\frac{\bar{D}_1^2/2}{d_0^2}, \tag{21}$$

where $\bar{D}_1^2/2$ is the mean square value of $\sum_\upsilon D_{\upsilon\upsilon}-D_{cc}$ for phonon pairs $(Qj,-Qj')$ in the spectral range ω_1 to ω_2, and n_p is

$$n_p=\frac{1}{N}\sum_{Qjj'}^{\omega_1<\omega_{Qj}+\omega Q_{j'}<\omega_2}f(Qjj'), \tag{22}$$

where $f(Qjj')$ is 0 for phonon pairs with small values of $\sum_\upsilon D_{\upsilon\upsilon}-D_{cc}$ and 1 for others. Since we observe both experimentally and theoretically that the Γ_1 Raman intensities resemble the overtone density of states (i.e., combinations $j'\neq j$ seem to be weak) we take $f=\delta_{jj'}$. Thus for the "2TO" band, $n_p\simeq 2$. In equation (21), ω_A and ω_B are the mean energies of the phonons ω_{Qj} and $\omega_{Qj'}$ in the band. The parameter $\frac{1}{2}\overline{D_1^2}$ has a factor of $\frac{1}{2}$ in its definition because the factor 2 in equation (8) was omitted in the experimental analysis summarized in Ref. 1, and we wish to remain consistent with past usage. For the TA+TO band $n_p=2$ is also taken in order to remain consistent with Ref. 1.

For E_0' gaps the analysis is similar and we use equation (21) with d_0 replaced by d_0–d_{15} to define a parameter $\overline{D_1^2}$ for E_0' gaps. For the $\Gamma_{25'}$ channel a similar analysis can be done. The corresponding deformation potentials $D_{25'}$ are defined in a way similar to d_0, since they have the same symmetry properties (see equation (2.241) of Ref. 1). We find for the function $A_{\Gamma_{25'}}(\omega_1,\omega_2)$ of a given spectral band:

$$A_{\Gamma_{25'}}(\omega_1,\omega_2)\cong\frac{8}{3}\left(\frac{\hbar}{M\omega_0 a^2}\right)\frac{\omega_0}{\omega_A}\frac{\omega_0}{\omega_B}\frac{3\overline{D_{25'}^2}/4}{d_0^2}$$
$$3\overline{D_{25'}^2}/4=\frac{1}{N}\sum_{\mathbf{Q}jj'}^{\omega_1<\omega_{\mathbf{Q}j}+\omega_{\mathbf{Q}j'}<\omega_2}D_{\upsilon 1,\upsilon 2}(\mathbf{Q}jj')^2. \tag{23}$$

We have listed in Table II the values of A (eq (20)) for several pairs of phonons from the calculations of Figs. 3–6. From these values of A we obtain the deformation potentials D listed in Table III. We have also listed in this table the experimental values of D obtained by an analogous procedure for similar gaps of

Table II

Ratios of second to first order scattering integrated over groups of phonons, A_{Γ_i} (see equation (20)) for Si and Ge near the E_0 and E_0' gaps, in units of 10^{-3}.

	E_0						E_0'					
	2TA		2TO		TA+TO		2TA		2TO		TA+TO	
	Γ_1	$\Gamma_{25'}$	Γ_1	$\Gamma_{25'}$	Γ_1	$\Gamma_{25'}$	Γ_1	$\Gamma_{25'}$	Γ_1	$\Gamma_{25'}$	Γ_1	$\Gamma_{25'}$
Si							2.0	0.6	78	3.3	4	1.2
Ge	1.1	0.3	17	4.4	1.4	0.8	0.8	0.3	45	5.3	3	1.0

Table III
Calculated and experimental values of second order electron–phonon deformation potentials D_1 and $D_{25'}$. Experimental data are from Table 2.11 of Ref. 1. The $D_{25'}$ for E_1 gaps have been obtained by dividing $D^5_{3,0}$ by $\sqrt{2}$ (see equation (2.200a) of Ref. 1).

	E_0				E_0'						E_1					
	2TA		2TO		2TA		2TO		TA+TO		2TA		2TO		TA+TO	
	Γ_1	$\Gamma_{25'}$	Γ_1	$\Gamma_{25'}$	Γ_1	$\Gamma_{25'}$	Γ_1	$\Gamma_{25'}$	Γ_1	$\Gamma_{25'}$	Γ_1	$\Gamma_{25'}$	Γ_1	$\Gamma_{25'}$	Γ_1	$\Gamma_{25'}$
Si, calc.					150	20	2800	160	360	50						
Si, exp.											80		1220	250		
Ge, calc.	100	14	1200	170	125	20	3000	280	490	80						
Ge, exp.											170		2534	350		
GaP	675		1670													
GaAs	170		2600								450		2070			100
ZnS	1600		2470													
ZnSe	545		510													
ZnTe	575		100													

other tetrahedral semiconductors. Comparison of theoretical with experimental D's is not straightforward since no equivalent gaps have been measured and calculated for the same material. Nevertheless one expects D_1(2TO) for the E_0 gap of Ge (theoretical) and GaAs or GaP (experimental) to be similar, a fact which is confirmed in Table III. Also, D_1(2TA) calculated for Ge is nearly the same as that measured for GaAs. One may also expect the D_1 for the E_0, E_0' (theory), and E_1 (experimental) in Ge and Si to be similar, a conjecture which is also confirmed in Table III. On this basis we consider the agreement between the theoretical and experimental data of Table III to be satisfactory. The failure to observe scattering by 2TA phonons in $\Gamma_{25'}$ configuration is explained by the small calculated values of the corresponding $D_{25'}$(2TA). It is hoped that this work will stimulate measurements of second order Raman scattering near the E_0 gap of Ge and also the more time-consuming calculations near the E_1 gaps near which experimental data for Ge and Si are available.

Acknowledgements

We would like to thank P. Lautenschlager for help with the numerical calculations. PBA thanks the Alexander von Humboldt–Stiftung for a senior US Scientist Award, and acknowledges partial support from NSF grant no. DMR 81–21954A01.

REFERENCES

[1] For a review see M. CARDONA, in *Light Scattering in Solids II*, ed. by M. Cardona and G. Güntherodt (Springer Verlag, Heidelberg, 1982), p. 19.
[2] B. A. WEINSTEIN and M. CARDONA, Phys. Rev. *B7*, 2545 (1973).
[3] P. A. TEMPLE and C. A. HATHAWAY, Phys. Rev. *B7*, 3685 (1973).
[4] W. WEBER, Phys. Rev. *B15*, 4789 (1977).
[5] M. A. RENUCCI, J. B. RENUCCI, R. ZEYHER, and M. CARDONA, Phys. Rev. *B10*, 4309 (1974).
[6] J. B. RENUCCI, R. N. TYTE, and M. CARDONA, Phys. Rev. *B11*, 3885 (1975).
[7] K. L. NGAI and E. J. JOHNSON, Phys. Rev. Letters *29*, 1607 (1972).
[8] S. GO, H. BILZ, and M. CARDONA, Phys. Rev. Letters *34*, 580 (1975); R. A. Cowley, J. Phys. *26*, 659 (1965).
[9] P. B. ALLEN and M. CARDONA, Phys. Rev. *B27*, 1495 (1981); *27*, 4760 (1983).
[10] M. L. COHEN and T. K. BERGSTRESSER, Phys. Rev. *141*, 789 (1966).
[11] G. E. JELLISON, JR., D. H. LOWNDES and R. F. WOOD, Phys. Rev. *B28*, 3272 (1983).
[12] L. VIÑA, S. LOGOTHETIDIS, and M. CARDONA, Phys. Rev., *B30*, 1979 (1984).
[13] B. CHAKRABORTY and P. B. ALLEN, Phys. Rev. *B18*, 5225 (1978).
[14] L. VIÑA and M. CARDONA, Phys. Rev., *B29*, 6739 (1984).
[15] A. K. GANGULY and J. L. BIRMAN, Phys. Rev. *162*, 806 (1967).
[16] P. LAWAETZ, Phys. Rev. *174*, 867 (1968).
[17] A. BLACHA, H. PRESTING, and M. CARDONA, Phys. Stat. Sol. (b), *b126*, 11 (1984).
[18] S. BEDNAREK and U. RÖSSLER, Phys. Rev. Letters *48*, 1296 (1982).